Shock and Vibration 19 (2012) 477–492
DOI 10.3233/SAV-2011-0644
IOS Press

Stress resultant based elasto-viscoplastic thick shell model

Pawel Woelke*, Ka-Kin Chan, Raymond Daddazio and Najib Abboud
Weidlinger Associates, New York, NY, USA

Received 24 April 2010
Revised 4 June 2011

Abstract. The current paper presents enhancement introduced to the elasto-viscoplastic shell formulation, which serves as a theoretical base for the finite element code EPSA (Elasto-Plastic Shell Analysis) [1–3]. The shell equations used in EPSA are modified to account for transverse shear deformation, which is important in the analysis of thick plates and shells, as well as composite laminates. Transverse shear forces calculated from transverse shear strains are introduced into a rate-dependent yield function, which is similar to Iliushin's yield surface expressed in terms of stress resultants and stress couples [12]. The hardening rule defined by Bieniek and Funaro [4], which allows for representation of the Bauschinger effect on a moment-curvature plane, was previously adopted in EPSA and is used here in the same form. Viscoplastic strain rates are calculated, taking into account the transverse shears. Only non-layered shells are considered in this work.

Keywords: Thick plates and shells, transverse shear deformation, elasto-viscoplastic analysis, rate dependent response

1. Introduction

Our objective is to introduce transverse shear strains and forces into the elasto-viscoplastic model of shell behavior, formulated within the finite element code EPSA. Only matters directly related to this objective are discussed in detail. For details of the finite element formulation, the reader is directed to references [1–4,8].

In our formulation, we use the following hypothesis: plane sections originally perpendicular to the middle surface remain plane after deformation but not perpendicular to the middle surface (Fig. 1). From this hypothesis, we deduce that bending displacements u and v along x and y directions are:

$$u = z\phi_x \text{ and } v = -z\phi_y \tag{1}$$

where ϕ_x and ϕ_y are the angles of rotation of the sections originally perpendicular to the middle section in the xz and yz planes, respectively, expressed by:

$$\phi_x = -\frac{\partial w}{\partial x} + \gamma_{xz} \text{ and } \phi_y = \frac{\partial w}{\partial y} - \gamma_{yz} \tag{2}$$

where w is the vertical displacement in the z direction and γ_{xz}, γ_{yz} are the transverse shear strains in the xz and yz planes, respectively.

Shells in which the ratio of the thickness to the radius of curvature is equal to or less than 1/50 are often considered thin (both lower and higher ratios are often used as an indication of shell thickness). In the case of thin shells, transverse shear strains are negligible. This is true for most boundary conditions. Some types of loading conditions, however, cause significant shear forces, regardless of the thickness of the structure. An example of such a loading condition is a concentrated bending moment applied at mid-span of the beam, plate, or shell (Fig. 2).

*Corresponding author. Tel.: +1 212 367 2983, ext: 3000; Fax: +1 212 497 2483; E-mail: woelke@wai.com; chan@wai.com.

ISSN 1070-9622/12/$27.50

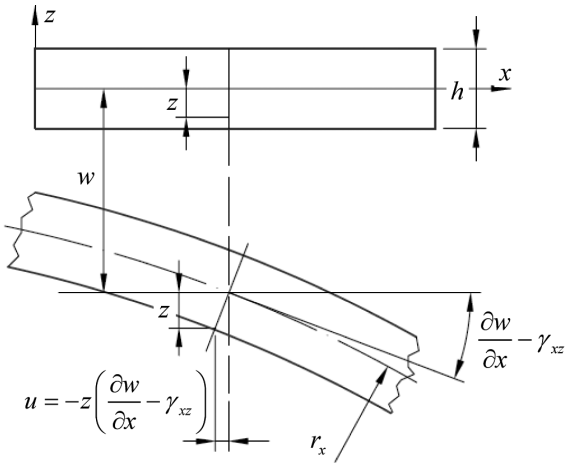

Fig. 1. Transverse shear deformations [24].

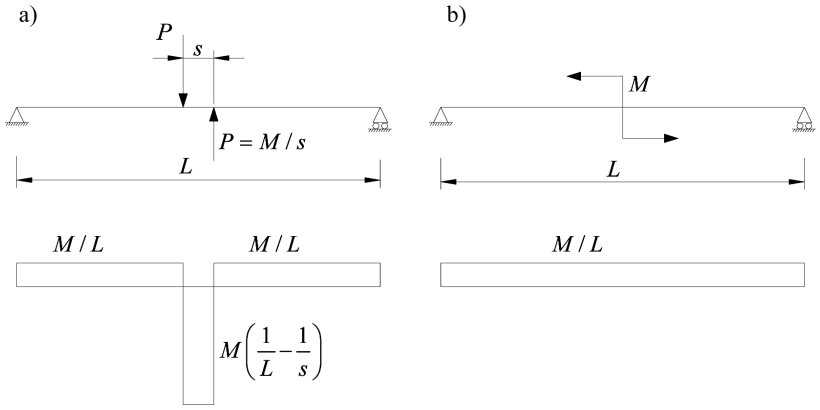

Fig. 2. Concentrated couples formed by: a) the vertical forces causing significant shear forces, and b) the horizontal forces – no significant shear forces [10].

The concentrated bending moment can be applied in two ways – by the vertical force couple (Fig. 2a) or by the horizontal force couple (Fig. 2b). With the former, a large shear force is generated at mid-span of the beam. The force increases as the distance between the forces s decreases. To correctly represent the beam deformation in this case, it is necessary to consider transverse shear strains, regardless of the beam thickness. The same situation occurs when such loading conditions are applied to plates and shells.

Transverse shear strains and forces are especially important in the analysis of composite laminates. Shear contributes significantly to delamination, a common failure mode in composites. In the current paper, only isotropic plates and shells are considered.

An Iliushin's yield function [12] modified to account for transverse shear forces, as well as the Bauschinger effect, is adopted. Transverse shear forces are known to significantly affect the plastic behavior of both thick and, under certain loading conditions, thin shells. Thus, shear forces are introduced into the yield function, in accordance with Shapiro's approach [20].

In the elasto-viscoplastic calculations, we follow the approach of Perzyna, who proposed a set of constitutive equations representing viscoplastic strain hardening for arbitrary loading histories [16]. The viscoplastic strain rate vector is directed along the normal to the subsequent dynamic yield surface. The quasi-static yield surface is defined in the stress resultant space (non-layered method), following an approach proposed by Iliushin [12]. Bieniek and Funaro [4] introduced hardening parameters into Iliushin's yield function in the form of residual bending moments, allowing for description of the Bauschinger effect on the moment-curvature plane. Voyiadjis and

Woelke [24] extended this idea, defining a three-dimensional kinematic hardening rule that uses not only residual bending moments, but residual normal and shear forces. We use Bieniek's and Funaro's definition of hardening parameters [4]. We modify the quasi-static yield surface to account for shear forces, as in Shapiro's approach [20].

Numerical integration of stresses through the thickness is not necessary with the non-layered formulation, making it less expensive computationally. Although the approximation of the yield criterion expressed in terms of forces and moments was expected to result in a loss of accuracy, this turned out not to be the case, as demonstrated by many authors who compared the two methods [1,21,24].

This paper is organized into six sections. Following the Introduction, Section 2 discusses the shell constitutive equations. Section 3 describes the finite element procedure. Section 4 defines the dynamic and quasi-static yield surface, flow, and hardening rules. Section 5 offers numerical examples, confirming that the current formulation provides good approximations. Section 6 presents the conclusion.

2. Shell constitutive equations

The plate or shell is assumed to be a solid, single-layer surface with thickness h (Fig. 1). The basic assumptions of the shell formulation are similar to those of Bieniek and Funaro [4]. At any point of the shell, the membrane strains and curvatures in a rectangular coordinate system (x, y, z) are expressed by the following equations:

$$e_x = \frac{\partial u_0}{\partial x} \tag{3}$$

$$e_y = \frac{\partial v_0}{\partial y} \tag{4}$$

$$e_{xy} = \frac{1}{2}\left(\frac{\partial u_0}{\partial y} + \frac{\partial v_0}{\partial x}\right) \tag{5}$$

$$\kappa_x = \frac{\partial \phi_x}{\partial x} = \frac{\partial}{\partial x}\left(-\frac{\partial w}{\partial x} + \gamma_{xz}\right) \tag{6}$$

$$\kappa_y = \frac{\partial \phi_y}{\partial y} = \frac{\partial}{\partial y}\left(\frac{\partial w}{\partial y} - \gamma_{yz}\right) \tag{7}$$

$$\kappa_{xy} = \frac{1}{2}\left(\frac{\partial \phi_x}{\partial y} + \frac{\partial \phi_y}{\partial x}\right) \tag{8}$$

The transverse shear strains are calculated using the following equations:

$$\gamma_{xz} = \frac{\partial w}{\partial x} + \phi_x \tag{9}$$

$$\gamma_{yz} = \frac{\partial w}{\partial y} - \phi_y \tag{10}$$

In Eqs (3)–(10) z is a measure of the distance between the middle surface of the shell and the surface under consideration (Fig. 1); e_x, e_y are membrane strains; e_{xy} is in-plane shear strain; $\kappa_x, \kappa_y, \kappa_{xy}$ are curvatures at the mid-surface in planes parallel to the xz, yz, and xy planes, respectively; u, v, w are the displacements along the x, y, z axes, respectively (Figs 1, 2); γ_{xz}, γ_{yz} are transverse shear strains in xz and yz planes (Fig. 1); and ϕ_x, ϕ_y are angles of rotation of the cross-sections normal to the mid-surface of the undeformed shell (Fig. 1).

The total normal strains due to both membrane and bending deformation in x, y directions, respectively, can be expressed as:

$$\varepsilon_x = e_x + z\kappa_x \quad \textit{and} \quad \varepsilon_y = e_y + z\kappa_y \tag{11}$$

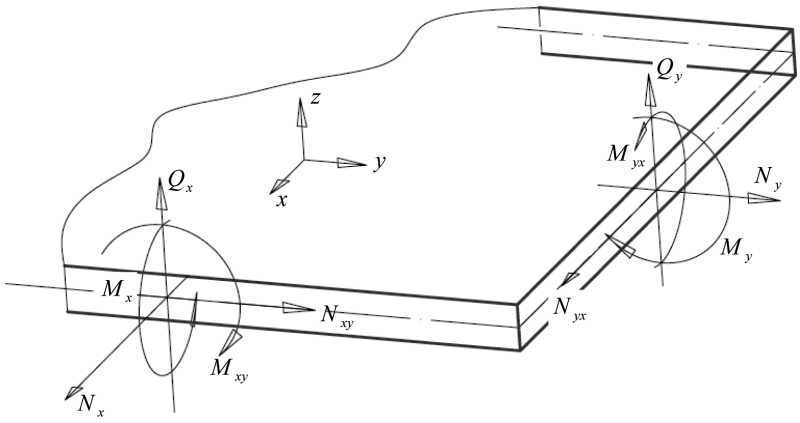

Fig. 3. Stress resultants on plate/shell element.

The stress resultants and couples $M_x, M_y, M_{xy}, N_x, N_y, N_{xy}, Q_x, Q_y$ shown in Fig. 3 can be expressed in terms of the strains given above:

$$M_x = D\left[\kappa_x + \nu\kappa_y\right] \tag{12}$$

$$M_y = D\left[\kappa_y + \nu\kappa_x\right] \tag{13}$$

$$M_{xy} = D\left(1-\nu\right)\kappa_{xy} \tag{14}$$

$$N_x = S\left[e_x + \nu e_y\right] \tag{15}$$

$$N_y = S\left[e_y + \nu e_x\right] \tag{16}$$

$$N_{xy} = S\left(1-\nu\right)e_{xy} \tag{17}$$

$$Q_x = T\gamma_{xz} \tag{18}$$

$$Q_y = T\gamma_{yz} \tag{19}$$

where:

$$D = \frac{Eh^3}{12\left(1-\nu^2\right)}, S = \frac{Eh}{\left(1-\nu^2\right)}, T = \frac{5}{12}\frac{Eh}{\left(1+\nu\right)} \tag{20}$$

and E is Young's Modulus, h is the shell thickness, and ν is Poisson's ratio. The positive directions of the stress resultants given by Eq (12)–(19) are shown in Fig. 3:

The above constitutive equations are universal for both plates and shells. The shell curvature is modeled through finite element discretization. When shear deformation is neglected, the constitutive Eqs (12)–(19) reduce to those given by Flugge [9].

3. Finite element formulation

The current element is a flat, constant-strain shell element with 4 nodes and 5 degrees of freedom per node, i.e., linear velocities $\dot{u}, \dot{v}, \dot{w}$ in x, y, z directions, respectively, and angular velocities $\dot{\phi}_x, \dot{\phi}_y$ around y and x axes, respectively. The positive directions of the degrees of freedom are the same as the positive directions of the stress resultants (Fig. 3).

Details of the kinematics of the element, solution of the equations of motion, time integration scheme, and anti-hourglassing procedure are available in references [1–4,8].

4. Rate-dependent yield function, flow, and hardening rules

As stated in the Introduction, we use a quasi-static yield criterion expressed in terms of stress resultants and couples, proposed by Iliushin [12] and modified by Bieniek and Funaro [4]. The following non-dimensional stress-resultant intensities are defined (Ref. [2,23–25]):

$$I_N = \frac{1}{N_0^2}\left(N_x^2 + N_y^2 - N_x N_y + 3N_{xy}^2\right) \tag{21}$$

$$I_M = \frac{1}{M_0^2}\left(M_x^2 + M_y^2 - M_x M_y + 3M_{xy}^2\right) \tag{22}$$

$$I_{NM} = \frac{1}{N_0 M_0}\left(N_x M_x + N_y M_y - \frac{1}{2}N_x M_y - \frac{1}{2}N_y M_x + 3N_{xy}M_{xy}\right) \tag{23}$$

$$I_{M^*} = \frac{1}{M_0^2}\left[\left(M_x - M_x^*\right)^2 + \left(M_y - M_y^*\right)^2 - \left(M_x - M_x^*\right)\left(M_y - M_y^*\right) + 3\left(M_{xy} - M_{xy}^*\right)^2\right] \tag{24}$$

$$N_0 = \sigma_0 h \quad and \quad M_0 = \frac{\sigma_0 h^2}{6} \tag{25}$$

σ_0 is the static one-dimensional yield strength and h is the shell thickness; M^* in Eq. (24) are hardening parameters to be defined.

The quasi-static yield surface is [2]:

$$F(\sigma) = I_N + I_N^2 - I_N^3 + I_{M^*} + 0.6\,|I_{NM}| \tag{26}$$

Equation (26) describes the current yield surface as the loading path moves from the initial yield surface $F_0(\sigma)$ toward a limit surface $F_L(\sigma)$. The initial yield surface represents the onset of yielding in the outer shell fibers and is expressed as:

$$F_0(\sigma) = I_N + I_M + 2\,|I_{NM}| \tag{27}$$

Time histories of vertical displacement (units – [in]) at point A due to triangular pulse load – with and without shear effects considered.

The limit yield surface represents the fully plastic cross section and is expressed as:

$$F_L(\sigma) = 2I_N - I_N^2 + \frac{4}{9}I_M \tag{28}$$

The hardening parameters M^* in equation (24) are now defined as [24]:

$$\begin{array}{l} if \quad F = 1 \quad and \quad \frac{\partial F}{\partial \sigma} d\sigma > 0 \\ dM_x^* = B_1\left(1 - F_L\right)\frac{M_0}{\kappa_0} d\kappa_x \\ dM_y^* = B_1\left(1 - F_L\right)\frac{M_0}{\kappa_0} d\kappa_y \\ dM_{xy}^* = B_2\left(1 - F_L\right)\frac{M_0}{\kappa_0} d\kappa_{xy} \\ if \quad F \leqslant 1 \quad or \quad \frac{\partial F}{\partial \sigma} d\sigma \leqslant 0 \quad then \quad dM_x^* = dM_y^* = dM_{xy}^* = 0 \end{array} \tag{29}$$

where $\kappa_0 = M_0/EI$ and E is Young's modulus, I is a second moment of area of the cross-section, and $B_1 = 9/5$ and $B_2 = 4/5$. These constants (B_1, B_2) were determined by comparison with the results obtained with the through-the-thickness integration technique described in Ref. [3].

Following the work of Shapiro [20], we account for the influence of shear forces on the plastic behavior of plates and shells. We can include transverse shear forces Q_x, Q_y by modifying one of the stress intensities, expressed by Eq. (21):

$$I_N = \frac{1}{N_0^2}\left[N_x^2 + N_y^2 - N_x N_y + 3\left(N_{xy}^2 + Q_x^2 + Q_y^2\right)\right] \tag{30}$$

The strain, stress resultants and hardening parameters (residual bending moments) are represented by 8x1 column matrices:

$$\begin{matrix}\mathbf{e}^T = \{e_x, e_y, e_{xy}, \kappa_x, \kappa_y, \kappa_{xy}, e_{xz}, e_{yz}\} \\ \mathbf{s}^T = \{N_x, N_y, N_{xy}, M_x, M_y, M_{xy}, Q_x, Q_y\}\end{matrix} \quad (\mathbf{s}^*)^T = \{0,\ 0,\ 0,\ 0,\ 0, M_{11}^*, M_{22}^*, M_{12}^*\} \tag{31}$$

Similarly, $\partial F/\partial \mathbf{s}$ is expressed as:

$$\left(\frac{\partial F}{\partial \mathbf{s}}\right)^T = \left\{\frac{\partial F}{\partial N_x}, \frac{\partial F}{\partial N_y}, \frac{\partial F}{\partial N_{xy}}, \frac{\partial F}{\partial M_x}, \frac{\partial F}{\partial M_y}, \frac{\partial F}{\partial M_{xy}}, \frac{\partial F}{\partial Q_x}, \frac{\partial F}{\partial Q_y}\right\} \tag{32}$$

We assume additive decomposition of the strain tensor into elastic and viscoplastic parts:

$$\mathbf{e} = \mathbf{e}^e + \mathbf{e}^{vp} \tag{33}$$

Following Perzyna's approach [16], Atkatsh et al. developed a generalization of the static yield surface to account for the strain-rate effects [2–4]. The viscoplastic strain rate tensor is assumed to depend on the stress resultant intensity through the associated flow rule:

$$d\mathbf{e}^{vp} = \gamma_R K \phi\left[F(\mathbf{s})\right] \frac{\partial F(\mathbf{s})}{\partial \mathbf{s}} = \bar{\lambda} \frac{\partial F(\mathbf{s})}{\partial \mathbf{s}} \tag{34}$$

where K is a work-hardening parameter describing deformation of the quasi-static yield surface during ineleastic processes [2–4] and γ_R and $\phi(F)$ are material response functions (γ_R is often taken as an inverse of viscosity determined for a given material). $\phi(F)$ is a Perzyna-type function defined as:

$$\phi(F) = \begin{cases} 0 & \text{for } F \leqslant 0 \\ \phi(F) & \text{for } F > 0 \end{cases} \tag{35}$$

By assuming that $\phi(F) = F$ and limiting Eq. (34) to a one-dimensional case, we can express the viscoplastic strain rate as:

$$d\mathbf{e}^{vp} = \frac{2}{\sqrt{3}} \gamma_R\ F\ \left(\sqrt{F+1}\right) \tag{36}$$

Using Eq. (29), the increment of hardening parameters (residual bending moments) can be written as:

$$d\mathbf{s}^* = A d\lambda \frac{\partial F}{\partial \mathbf{s}'} \quad \text{where} \quad A = \beta \frac{M_o}{\kappa_o} \quad \text{and} \quad \mathbf{s}' = \{0, 0, 0, 0, 0, M_{11}, M_{22}, M_{12}\} \tag{37}$$

Applying the following elastic law:

$$\mathbf{s} = \mathbf{E}\left(\mathbf{e} - \mathbf{e}^{vp}\right) \tag{38}$$

and Eq. (34), we can express the viscoplastic multiplier $\bar{\lambda}$ as:

$$\bar{\lambda} = \frac{\left(\frac{\partial F}{\partial \mathbf{S}}\right)^T \mathbf{E} d\mathbf{e}}{\left(\frac{\partial F}{\partial \mathbf{S}}\right)^T \mathbf{E} \frac{\partial F}{\partial \mathbf{S}} - \left(\frac{\partial F}{\partial \mathbf{S}^*}\right)^T A \frac{\partial F}{\partial \mathbf{S}'}} \tag{39}$$

where Δt is a time increment, $\mathbf{s}^{\mathbf{e}}$ is the elastic stress vector, and $\mathbf{E}$ is the elastic shell stiffness matrix defined by Eqs (12)–(20). Because Eq. (39) cannot be solved directly for $\bar{\lambda}$, we solve the equivalent form:

$$\bar{\lambda} = \left[\gamma_R,\ \Delta t,\ K,\ \mathbf{E},\ F\left[\left(\mathbf{S}^{\mathbf{e}}\right)^T\right],\ \frac{\partial F}{\partial \mathbf{S}}\right] = 0 \tag{40}$$

using an iterative modified falsi method [1–4].

Functions γ_R and $\phi(F)$ can be selected to fit experimental test results of the dynamic behavior of a particular material. Available experimental methods include a one-dimensional stress-strain test using a Hopkinson bar technique [14]. γ_R should be calibrated to adequately represent the results of a multiaxial test on plate and shell specimens. The experiments should consist of biaxial bending and stretching tests conducted at various loading rates. The current lack of experimental data precludes choosing function γ_R to fit measured results. Thus, γ_R

was selected such that the stress resultants correspond to those obtained using a layered (through-the-thickness integration) method [1–4].

For mild steel [7] the proposed function γ_R takes the form [1–4]:

$$\gamma_R = \frac{a_1}{F^{n_1}\left(F_L - F\right)^{n_2}} \tag{41}$$

where F and F_L are for one-dimensional cases as in [1–4]:

$$F = \left(\frac{\sigma}{\sigma_0}\right)^2 - 1 \quad ; \quad F_L = \left(\frac{\sigma_{LIM}}{\sigma_0}\right)^2 - 1 \tag{42}$$

Material constants a_1, n_1, n_2 were determined for mild steel:

$$a_1 = 30.0; \;\; n_1 = 0.75; \;\; n_2 = 0.25 \tag{43}$$

5. Numerical examples

The reliability of these concepts is verified through a set of discriminating examples. The problems are selected to challenge new features introduced into the finite element code EPSA, i.e., representation of shear deformation and shear forces in the elasto-viscoplastic shell model. The importance of shear deformation in the analysis of thick shells is widely known and has been discussed by many authors. The reliability of rate-dependent formulation has also been confirmed [1–4]. The objective of this section is to confirm that the description of shear effects presented here is reliable and capable of correctly modeling elasto-viscoplastic behavior of thick plates and shells. Both beam and shell problems, simulated with shell elements are used to show the reliability of presented formulation. Although the current work discusses shell element formulation, beams problems (modeled with shell elements) are convenient for verification, since the analytical solutions which serve as references, can be easily established. We note that despite the geometric simplicity of the beam examples, the boundary conditions are chosen such that the problems present challenging tests for accuracy of the new features of the presented shell formulation, i.e. representation of the shear deformation. The last example considers a cylindrical shell with varying thickness, which allows for investigation of the increasing importance of the shear deformation with increasing thickness of the shell.

5.1. Simply supported beam subjected to a force couple at mid-span

We consider here the simply supported beam discussed in the Introduction. The geometry of the beam, as well as the shear forces and bending moment diagrams, are given in Fig. 8.

The length of the beam is $L = 10\ in$, the distance between the forces $s = 0.625\ in$, $P = 100\ lb$, $M = 62.5\ lb\ in$, Young's modulus is $E = 3.0 \times 10^7\ psi$, and the cross section of the beam is rectangular with $b = h = 1.0\ in$. The flexural and shear rigidities of the beam are obtained by Eq. (20) with $\nu = 0$, $D = 25 \times 10^5\ lb\ in^2$, and $T = 125 \times 10^5\ lb$.

As noted in the Introduction, there is a significant difference between applications of the concentrated bending moment formed by a vertical force couple and those formed by a horizontal one. When distance s is very small, the bending moment diagrams in (Figs 8a and 8b) are almost identical, but the shear force diagrams are different. For the example in (Fig. 8a), there is a very large shear force between points A and B. If the classical (thin shell) formulation is applied, the difference in shear force is immaterial [10]. In reality, however, the shear force causes additional strains in the beam, which lead to increased vertical displacement, as well as discontinuity of the displacement function between points A and B. Only the thick shell formulation, which takes into account transverse shear deformation, is capable of correctly predicting shear effects and vertical displacements in points A and B.

We will confirm that the current formulation features reliable representation of shear effects and is therefore applicable to the analysis of thick shells. First we analytically calculate vertical displacement at point A for both loading cases in (Fig. 4a and 4b), considering the influence of bending moments and shear forces (thick beam theory). We will refer to the boundary conditions in Fig. 4 a) as "case a" and Fig. 4 b) as "case b." We apply the virtual unit force at point A, as shown in Fig. 7, to determine the displacement by means of the virtual work principle.

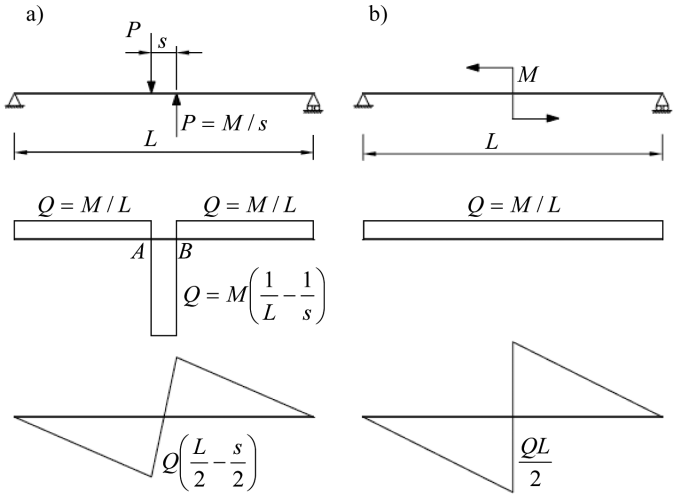

Fig. 4. Simply supported beam subjected to concentrated couples formed by, a) the vertical forces causing significant shear deformation, and b) the horizontal forces – no significant shear deformation [10].

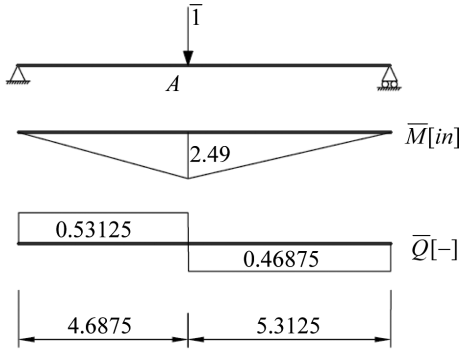

Fig. 5. Simply supported beam subjected to a virtual displacement unit force at point A, virtual bending moment $\bar{M}$, and shear force $\bar{Q}$ diagram.

The vertical displacement at point A, due to bending moment and shear force, is expressed by:

$$w = w_M + w_Q = \int_L \frac{M\bar{M}}{D} dx + \int_L \frac{Q\bar{Q}}{T} dx \tag{44}$$

where w_M and w_Q are vertical displacements at point A due to bending moments and shear forces, respectively; $\bar{M}$ and $\bar{Q}$ are virtual bending moment and shear force, as shown in Fig. 7; and M and Q are real bending moment and shear force in the beam.

The integral in Eq. (44) can be calculated using Simpson's rule or the Mohr-Wereszczegin method. For "case b" the vertical displacement $w^b = w_M^b + w_Q^b$ at point A is obtained by:

$$w^b = w_M^b + w_Q^b = \frac{14.74}{D} + \frac{0.0}{T} = 5.896 \times 10^{-6}\ in \tag{45}$$

It is important to note that for "case b" the influence of shear forces is 0. This means that the thin shell formulation, which does not account for transverse shear deformation, produces accurate solutions for the displacement of the beam only for "case b."

The vertical displacement for "case a" is:

$$w^a = w_M^a + w_Q^a = \frac{14.29}{D} + \frac{29.297}{T} = 8.056 \times 10^{-6}\ in \tag{46}$$

Table 1
Comparison of results (all values at point A)

	Analytical 'case a'	EPSA 'case a'	Analytical 'case b'	EPSA 'case b'
Displacement [in]	8.056×10^{-6}	7.9704×10^{-6}	5.896×10^{-6}	5.912×10^{-6}
Shear force [lb]	-93.75	-93.75	6.25	6.25
Bending moment [lb in]	29.30	28.32	29.30	28.32

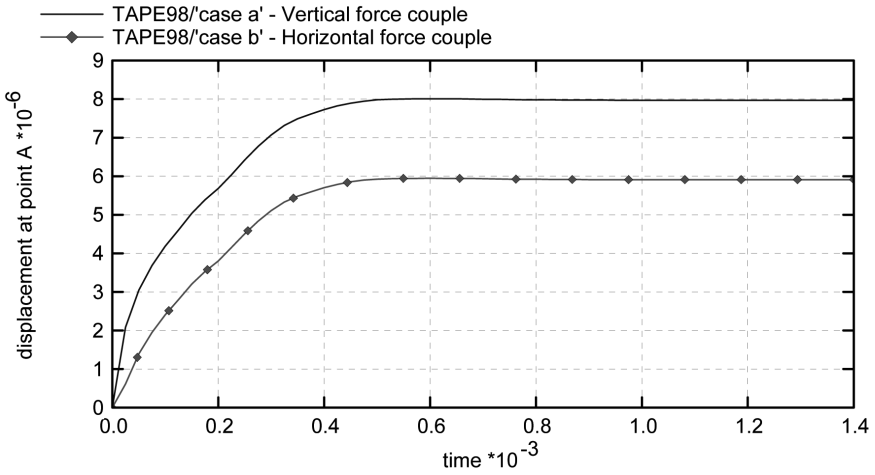

Fig. 6. Displacement time histories (units – [in]) for "case a" and "case b". (Displacement at point A: $w = w_M + w_Q$)

The influence of bending moments is almost identical for both "case a" and "case b." This is to be expected, as the bending moment diagrams in Fig. 4 a) and 4 b) are almost identical. As the distance s decreases, the displacement due to bending moment in "case a" approaches that of "case b." The difference in the results in Eqs (45) and (46) is caused by the influence of the large shear force induced by application of the force couple, as shown in Fig. 4 a). The shear deformation accounts for almost 30% of the total displacement at point A. This difference, which is significant, can be calculated correctly only by use of a reliable thick shell formulation.

The problem described above is modeled using an EPSA code with 32 thick shell elements and the results compared with the above analytical results. Figure 6 presents the time history for the vertical displacement at point A (Fig. 8) for cases "a" and "b":

Table 1 compares the analytical and numerical values of vertical displacement, shear force, and bending moment at point A:

Figure 6 and Table 1 show that results obtained using EPSA compare well with the analytical results. Most important, in "case a" the vertical displacement caused by bending and shear actions is approximated correctly. This confirms that EPSA features reliable representation of transverse shear deformation and can be used successfully to model the elasto-plastic behavior of thick plates, shells, and beams.

In elasto-viscoplastic analysis, if the loading is applied very slowly, one approaches a rate-independent response. In other words, if rate-dependent and rate-independent models are used separately to analyze the same problem and the loading is applied very slowly for the rate-dependent model, the results should be approximately the same. If this is so, then provided that the shear representation in the rate-independent model is reliable, shear representation in the rate-dependent model should also be reliable. Considering the above argument, we subject the simply supported beam to a vertical force-couple and analyze the problem separately by means of elasto-plastic and elasto-viscoplastic formulations. The static yield stress is $\sigma_0 = 190\ ksi$ and the dynamic yield stress is $\sigma_{LIM} = 195\ ksi$. A slow rate of loading in the viscoplastic model and small difference between static and dynamic yield stresses suggest a response that is practically rate-independent. Time histories for transverse shear force, bending moment, and vertical displacement at point A, calculated using both rate-independent and rate-dependent approaches, are shown in Fig. 7.

We see in Fig. 7 that the results obtained using EPSA rate-independent and rate-dependent formulations, with small strain rate hardening in the latter, match almost exactly. As the rate–independent formulation features reliable

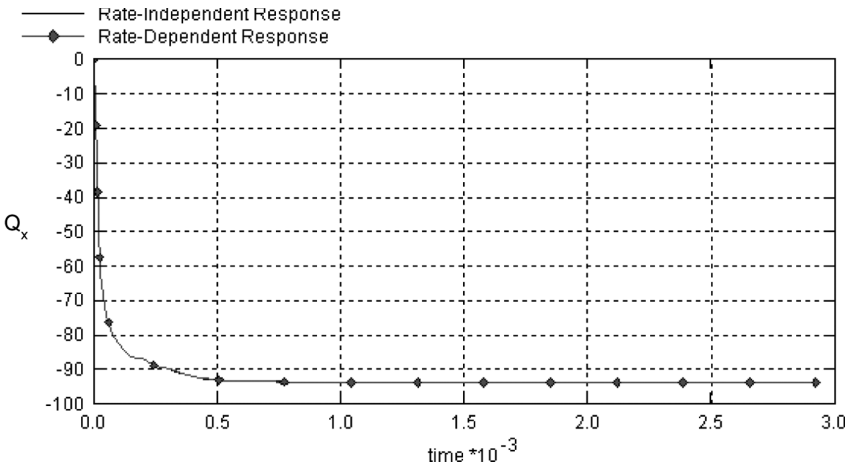

a) Time history of shear force at point A (units [lb])

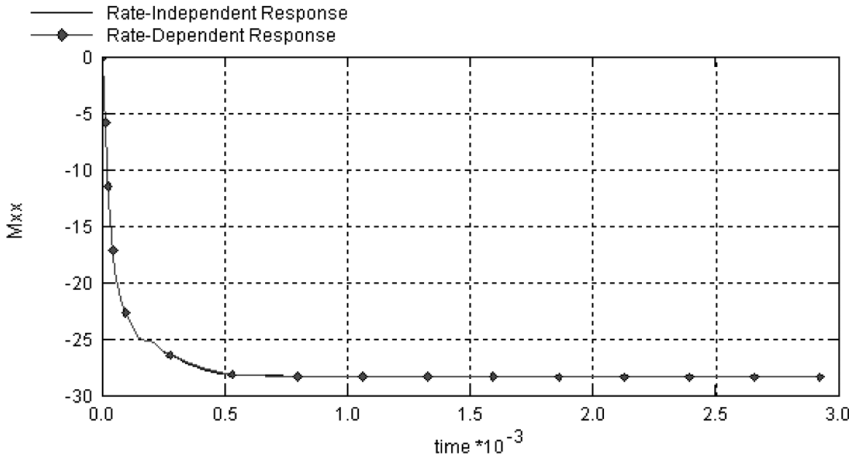

b) Time history of bending moment at point A (units [lb-in])

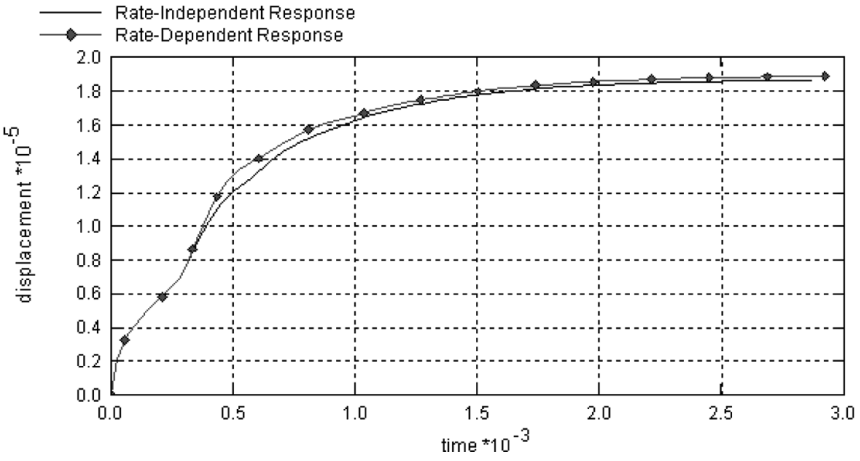

c) Time history of vertical displacement at point A (units [in])

Fig. 7. Time histories of: a) transverse shear force, b) bending moment, and c) vertical displacement at point A, calculated using rate-independent and rate-dependent approaches.

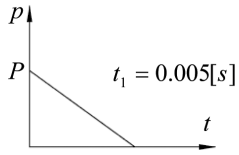

Fig. 8. Loading time history – triangular pulse load.

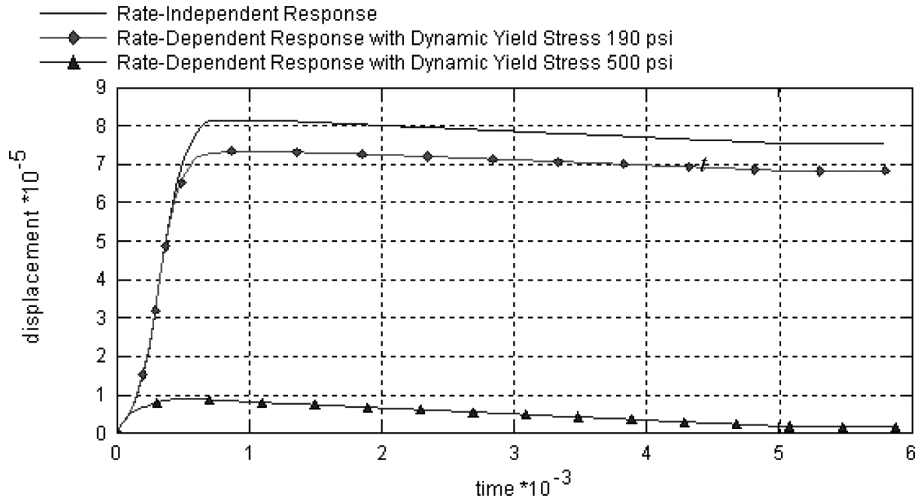

Fig. 9. Time histories of vertical displacement (units – [in]) at point A due to triangular pulse load.

representation of shear effects, as verified in Ref. [2–4], we conclude that the shear effects are also correctly described in a rate-dependent model. Thus, the elasto-viscoplastic formulation is applicable to the analysis of both thick and thin beams, plates, and shells.

We also investigate the strain rate effects in the context of the above problem, with a triangular pulse loading function applied, as shown in Fig. 8. To ensure the presence of permanent deformation, we lower the static yield stress to $\sigma_0 = 160\ ksi$. Two cases of dynamic yield stresses in the elasto-viscoplastic model are considered, $\sigma_{LIM} = 190\ ksi$ and $\sigma_{LIM} = 500\ ksi$. We expect the results of the elasto-plastic and elasto-viscoplastic analyses with $\sigma_{LIM} = 190\ ksi$ to be similar and observe significant strain rate hardening when $\sigma_{LIM} = 500\ ksi$. The displacement time histories for the three cases are shown in Fig. 9.

Figure 9 shows relatively small differences between the rate-independent and rate-dependent responses with dynamic yield stress $\sigma_{LIM} = 190\ ksi$. This difference is attributed to strain rate hardening, resulting in a reduced permanent deflection. The effect of strain rate hardening is more prominent with the higher dynamic yield stress $\sigma_{LIM} = 500\ ksi$.

To confirm the importance of shear effects in the viscoplastic analysis, we compare the vertical displacement at point A, calculated using elasto-viscoplastic representation, with dynamic yield stress $\sigma_{LIM} = 500\ ksi$, both taking shear forces into account (Eq. (30)) and not taking them into account (Eq. (21)). The displacement time histories are given in Fig. 10.

The displacement obtained using the thick shell formulation is substantially larger than that obtained using the thin shell formulation (Fig. 10). Moreover, there is no permanent deformation when shear forces are ignored. It is therefore important to include shear effects in the analysis of thick structures.

The results in Fig. 10 indicate that that presented description of shear deformation is well grounded.

5.2. Elasto-plastic simply supported beam

The importance of transverse shear forces in approximations of the collapse load of thick beams, plates, and shells is known to be significant. Accurate and safe approximations should result in a decreasing value of the maximum

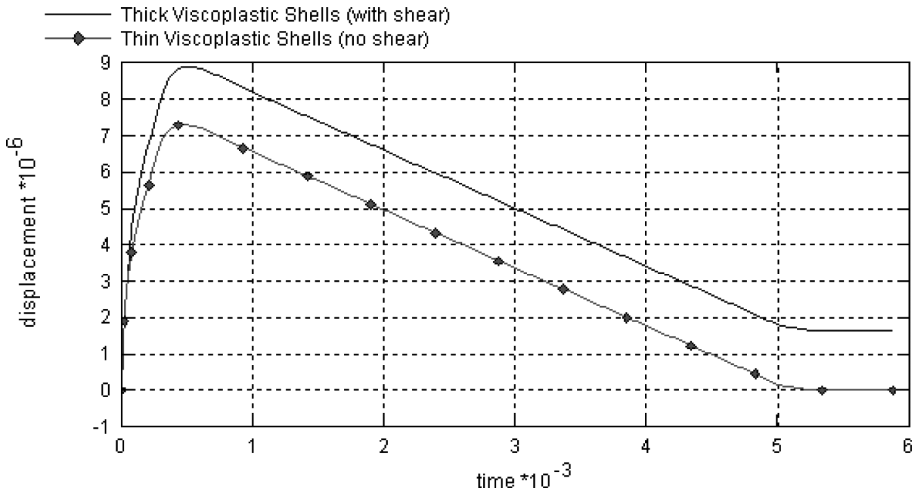

Fig. 10. Time histories of vertical displacement (units – [in]) at point A due to triangular pulse load – with and without shear effects considered.

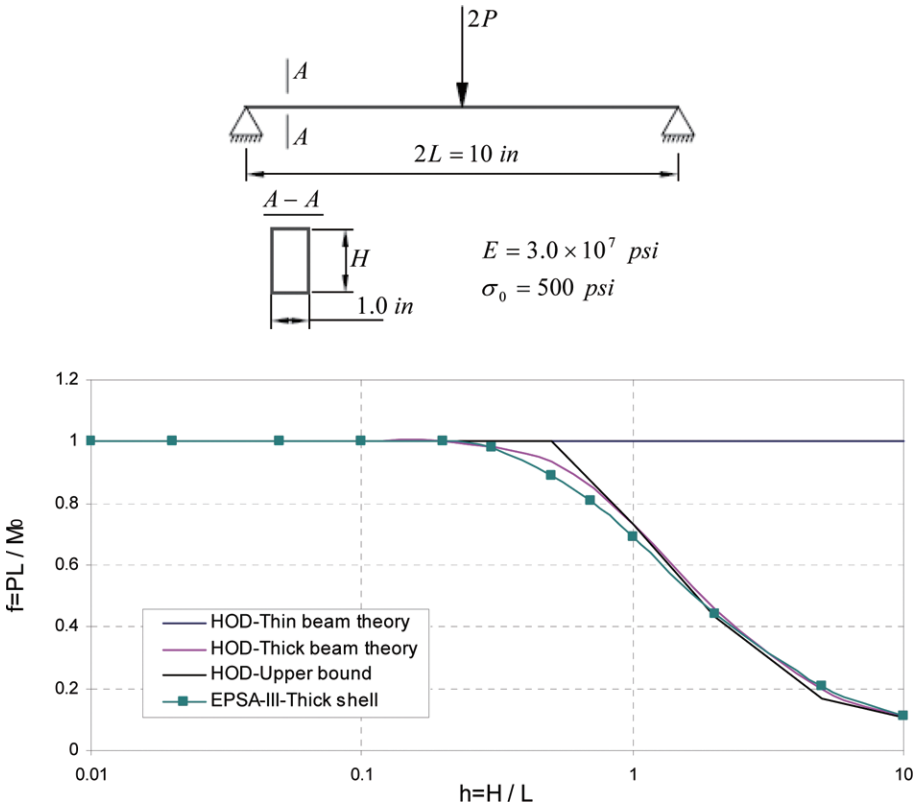

Fig. 11. Simply supported beam – geometry, material properties, and results; collapse load as a function of thickness (HOD-Hodge [11]).

load factor with increasing thickness. To test the accuracy of our formulation in accounting for shear deformation, we consider a simply supported beam of length $2L = 10\ in$, subjected to a concentrated load $2P$ at its mid-point. Young's modulus is $E = 3.0\ x\ 10^7\ psi$, the yield stress is $\sigma_0 = 500\ psi$, and the width of the beam is $b = 1\ in$ (Fig. 11). As in the previous example, we model the beam with 32 thick shell elements using EPSA and compute the load factor of the beam as a function of its thickness. The analytical solution of this problem given by Hodge [11]

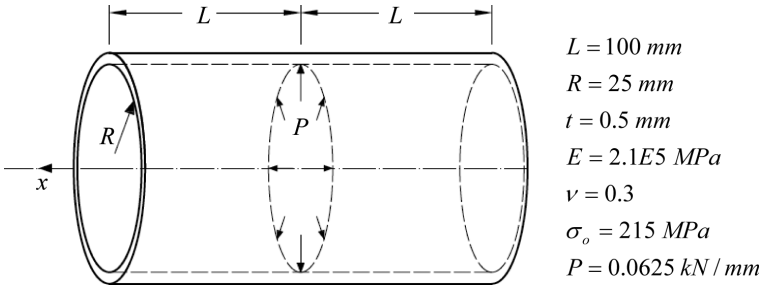

Fig. 12. Cylindrical shell subjected to a ring of pressure.

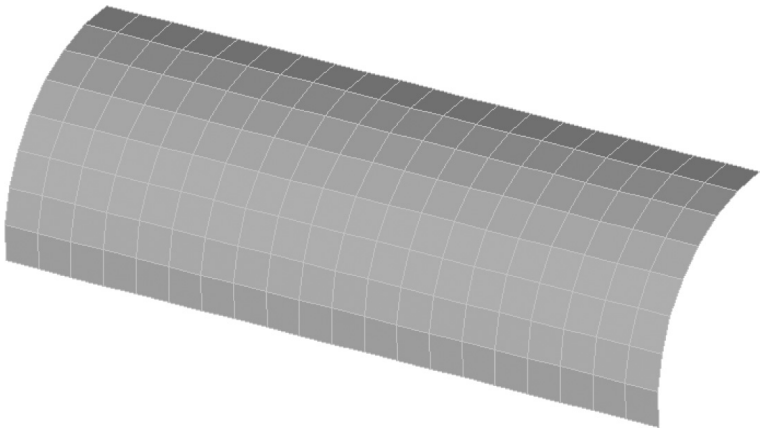

Fig. 13. Finite element mesh of an octant of the cylinder.

serves as a reference solution.

As seen in Fig. 11, the results obtained with the EPSA thick shell element closely agree with the analytical results of Hodge [11]. As expected, there is a substantial reduction in the collapse load factor for thick beams. This confirms that our representation of shear effects in the elasto-plastic analysis of shells is sound and capable of delivering accurate results.

For practical purposes, only a certain range of H is significant. When the thickness of the beam, plate, or shell exceeds 50% of its total length, the problem becomes purely academic, although it is still valuable for illustrative purposes.

5.3. Cylindrical shell subjected to a ring of pressure

As discussed in the Introduction, the main objective of the current work is to account for the influence of transverse shear strains and stresses on the behavior of shell structures subjected to static and dynamic loads. To further verify the dependability of the representation of the transverse shear effects, we consider a cylindrical shell under the ring of pressure. The geometry and material parameters are shown in Fig. 12. Due to symmetry, we only consider an octant of the shell, which is modeled using finite element mesh, as shown in Fig. 13.

We analyze the problem using EPSA shell elements, based on the thin shell formulation, and compare the results with those obtained using the same shell elements modified to account for transverse shear deformation. First, we consider a cylinder with thickness $t = 0.5$ mm. Shells in which the ratio of the radius of the curvature and thickness is higher than 50 usually are considered thin. In this case, the results delivered by EPSA thin-layered shell element, previously shown to be reliable, will be sufficiently accurate. Solving the problem using the thick layered shell formulation presented here should therefore produce similar results. We compare the radial displacements at midspan of the cylinder, determined by thin and thick shell formulations. The time history plots are shown in Fig. 14.

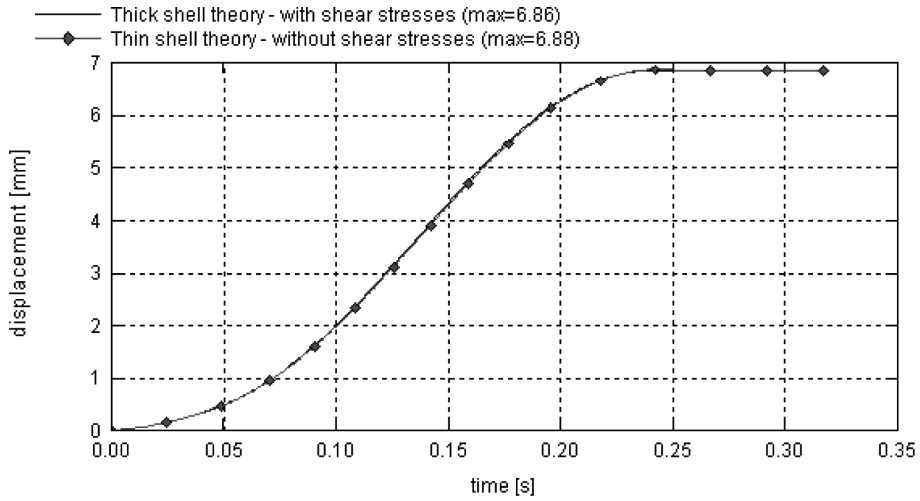

Fig. 14. Radial displacements for a cylinder subjected to a ring of pressure ($t = 0.5\ mm$).

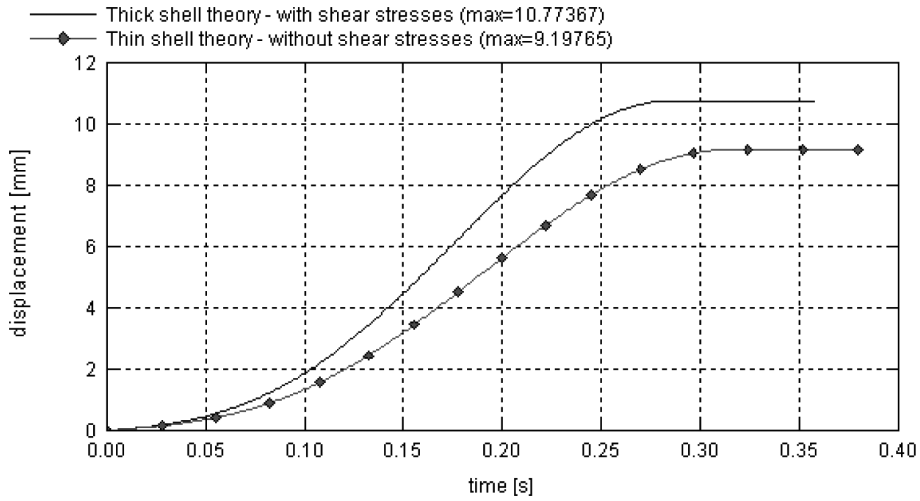

Fig. 15. Radial displacement for a cylinder subjected to a ring of pressure ($t = 5$ mm).

Figure 14 shows that, as expected, the results produced by the thin and thick shell formulations are practically identical. Shear effects are negligible in this problem, as correctly recognized by the thick shell model.

We increase the thickness of the cylinder to $t = 5\ mm$ and the pressure to $P = 1.0\ kN/mm$ and again compare the radial displacements obtained from the two formulations. The displacement time history plots are shown in Fig. 15.

Displacement calculated using the current, thick shell formulation is 17% larger than that obtained without accounting for shear stresses. At the same time, the bending moments and axial forces determined by the thick and thin shell formulations are approximately the same (Fig. 16). This significant discrepancy between displacement values is attributed to increased influence of the transverse shear effects, which are correctly represented in the current formulation.

6. Conclusion

We introduce transverse shear effects into a viscoplastic model formulated using the finite element code EPSA. Accounting for out-of-plane shear strains and stresses is necessary for accurate modeling of the elastic and plastic,

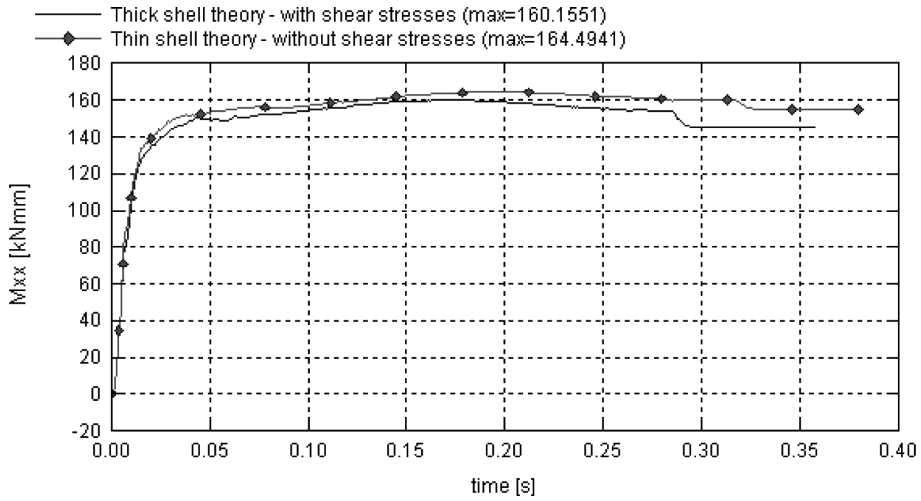

Fig. 16. Bending moment at midspan of the cylinder subjected to a ring of pressure ($t = 5$ mm).

rate-dependent behavior of thick plates and shells. A stress-resultant-based, dynamic yield surface is used, with shear forces calculated from transverse shear strains.

EPSA is an explicit code featuring a constant strain shell element. The equation of motion is solved locally, without assembling the stiffness matrix of the structure. Neither shear nor membrane locking is experienced here. The description of the solution procedure of the dynamic equations of motion, as well as the anti-hourglass procedure and other details of he code are discussed in references [1–4,8].

The numerical examples were selected to challenge the most important feature of this work, the representation of transverse shear effects in elasto-viscoplastic investigations. The beam problems were solved using shell elements with elasto-plastic and elasto-viscoplastic material representations. The boundary conditions and material properties were set such that the problem is a discriminating test of the accuracy of the formulation with respect to description of the shear effects in the viscoplastic shell model.

In all the cases considered, the calculated responses of the structure showed that the formulation is well grounded. The EPSA rate-dependent shell finite element is therefore capable of producing accurate approximations of elastic and elasto-viscoplastic behavior of thin and thick beams, plates, and shells.

References

[1] R.S. Atkatsh, M.L. Baron and M.P. Bieniek, A Finite Difference Variational Method for Bending of Plates, *Computers & Structures* **11** (1980), 573–577.
[2] R.S. Atkatsh, M.P. Bieniek and M.L. Baron, Dynamic Elasto-Plastic Response of Shells in an Acoustic MediumZ – EPSA Code, *Int J Num Meth Eng* **19**(6) (1983), 811–824.
[3] R.S. Atkatsh, M.P. Bieniek and I.S. Sandler, Theory of Viscoplastic Shells for Dynamic Response, *J of Applied Mechanics* **50** (1983), 131–136.
[4] M.P. Bieniek and J.R. Funaro, *Elasto-Plastic Behavior of Plates and Shells*, Technical report DNA 3584A, Weidlinger Associates, New York, 1976.
[5] E.D. Bingham, *Fluidity and Plasticity*, McGraw-Hill, 1922.
[6] S.R. Bodner and Y. Partom, Constitutive Equations for Elastic-Viscoplastic Strain-Herdening Materials, *J Appl Mech June* (1975), 385–389.
[7] D.S. Clark and P.E. Duwez, The influence of Strain Rate on Some Tensile Properties of Steel, *Proc Am Soc Testing Materials* **50** (1950), 560–575.
[8] D.P. Flanagan and T. Belytschko, A uniform strain hexahedron and quadrilateral with orthogonal hourglass control, *Int J Num, Meth Eng* **17** (1981), 679–706.
[9] W. Flugge, *Stresses in Shells*, Springer, New York, 1960.
[10] H.-C. Hu, *Variational Principles of Theory of Elasticity with Applications*, Scientific Publisher, Beijing, China, 1984.
[11] P.G. Hodge, *Plastic Analysis of Structures*, McGraw-Hill, 1959.
[12] A.A. Iliushin, Plastichnost', Gostekhizdat, Moscow, 1956.

[13] W.B. Kratzig, 'Best' transverse shearing and stretching shelll theory for nonlinear finite element simulations, *Comp Meth Appl Mech Eng* **103** (1992), 135–160.
[14] U.S. Lindholm, *Review of Dynamic Testing Techniques and Material Behavior*, Conference on Mechanical Properties of Materials at High Rates of Strain, Institute of Physics, London, 1974.
[15] E. Onate, A review of some finite element families for thick and thin plate and shell analysis, in: *Recent Developments in FE Analysis*, T.J.R. Hughes, E. Onate, and O.C. Zienkiewicz, eds, CIMNE: Barcelona, 1999.
[16] P. Perzyna, Fundamental Problems in Viscoplasticity, *Advances in Applied Mechanics* **9** (1966), 243–377.
[17] E. Reissner, The effects of transverse shear deformation on the bending of elastic plates, *J Appl Mech ASME* **12** (1945), 66–77.
[18] E. Reissner, On transverse bending of plates, including the effects of transverse shear deformation, *Int J Solids Structures* **11** (1975), 569–576.
[19] M. Robinson, A comparison of yield surfaces for thin shells, *Int J Mech Sci* **13** (1971), 345–354.
[20] G.S. Shapiro, On yield surface for ideally plastic shells. In Problems of Continuous Mechanics, SIAM, Philadelphia, 1961, 414–418.
[21] G. Shi and G.Z. Voyiadjis, A simple non-layered finite element for the elasto-plastic analysis of shear flexible plates, *Int J Num Meth Engng* **33** (1992), 85–99.
[22] J.C. Simo, D.D. Fox and M.S. Rifai, On a stress resultant geometrically exact shell model, *Part II: The linear Theory* **73** (1989), 53–92; *Part III: Computational Aspects of the Nonlinear Theory* **79**, 21–70. Computer Methods in Applied Mechanics and Engineering. North-Holland.
[23] P. Woelke, G.Z. Voyiadjis and P. Perzyna, Elasto-plastic finite element analysis of shells with damage due to microvoids, *Int J Num Meth Eng* **68**(3) (2006), 338–380.
[24] G.Z. Voyiadjis and P. Woelke, General non-linear finite element analysis of thick plates and shells, *Int J Solids Structures* **43**(Issue 7–8, 1) (2005), 2209–2242.
[25] G.Z. Voyiadjis and P. Woelke, (2009), *Elasto-Plastic and Damage Analysis of Plates and Shells*, Springer 2008.
[26] G.A. Wempner, *Nonlinear Theory of Shells*, ASCE National Environmental Engineering Meeting, New York, 1973.